ISSN 0015-4628, Fluid Dynamics, 2016, Vol. 51, No. 6, pp. 804–813. © Pleiades Publishing, Ltd., 2016.
Original Russian Text © E.I. Vasil'ev, 2016, published in Izvestiya Rossiiskoi Akademii Nauk, Mekhanika Zhidkosti i Gaza, 2016, Vol. 51, No. 6, pp. 91–100.

The Nature of the Triple Point Singularity in the Case of Stationary Reflection of Weak Shock Waves

E. I. Vasil'ev

Volgograd State University, pr. Universitetskii 100, Volgograd, 400062 Russia

e-mail: vas44il@gmail.com

Received February 16, 2016

Abstract—The structure of flow in the vicinity of a triple point in the problem of stationary irregular reflection of weak shock waves is numerically investigated within the framework of the Euler model, including the von Neumann paradox range. To improve the accuracy of the solution near singular points a new technology including a grid contracted toward the triple point and the discontinuity fitting is applied. It is shown that in the four-wave flow pattern the curvatures of the tangential discontinuity and the Mach front at the triple point are finite. The singularity is concentrated only in a sector between the reflected wave front and the expansion fan. When the three-wave flow pattern is realized, the curvatures of the tangential discontinuity and both wave fronts at the triple point are infinite. On the range of weak and moderate shock waves the logarithmic singularity in subsonic sectors near the triple point conserves up to transition to the regular reflection.

Keywords: irregular reflection, triple pont, von Neumann paradox, logarithmic singularity, discontinuity fitting.

DOI: 10.1134/S0015462816060119

The problem of weak Mach-type shock wave reflection in an ideal gas called the von Neumann paradox or the triple point paradox was successfully solved at the end of the last century. In [1–3] it was shown that on the range of the relevant parameters, at which the solution of the classical problem based upon three-shock theory is absent from the triple point vicinity, it is the four-wave flow configuration with a centered expansion wave and a local supersonic zone suggested by Guderley as long ago as in 1947 [4] that is realized. Later the four-wave flow configuration was found in the experiments in a shock tunnel of large cross-section [5, 6] and of standard section [7]. On the range of very weak reflected waves, in some experiments [6, 7] and numerical calculations [8] a cascade of several supersonic zones closed by deceleration shocks was found to exist, additionally to the four-wave configuration. Quite recently, the cascade structure of the supersonic region behind a triple point was confirmed also for moderately weak reflections [9, 10].

In [3] it was analytically shown that in the four-wave configuration the reflected front possesses the logarithmic singularity with infinite curvature at the triple point. An analogous property for the Mach front and the tangential discontinuity remained open question.

In this study, these and some other questions are numerically investigated using a more accurate technique with reference to the problem of stationary reflection of an oblique shock wave in a plane supersonic flow of an ideal perfect gas (Fig. 1). The diagram of possible triple-point configurations (T-configurations) in the plane of the parameters M_0 and β is plotted in Fig. 2 for a small range of moderately weak shock waves. The letter designations of the regions are taken from book [11]. In the regions above curve *1* and below curve *6* there is no reflection. In the region below curve *6* the incident shock does not exist, since $M_n = M_0 \sin\beta < 1$, while in the region above curve *1* the flow behind the incident shock is subsonic, so that the reflected shock does not exist. Regions *2* and *3* (GR and VR) form the von Neumann paradox region,

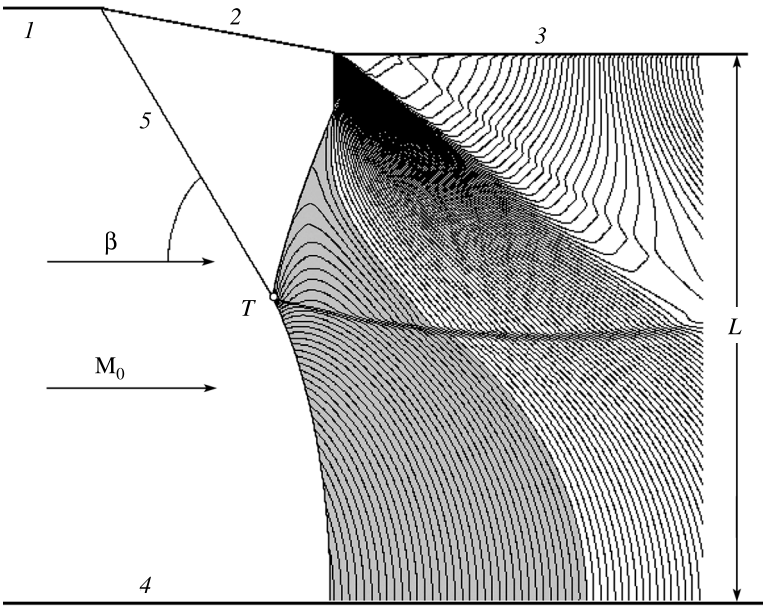

Fig. 1. Steady irregular reflection of a shock wave in a plane channel. Density contours for a case with a non-maximum Mach front height; (*1–4*) are the channel walls and (*5*) is the front of the incident shock wave inclined by an angle β to the oncoming flow with the Mach number M_0; L is the height of the narrow section of the channel.

where the three-wave T-configuration is replaced by the four-wave flow configuration near the triple point. In the regions located below curve *3* there exist solutions in the form of three-wave (vNR and MR) and two-wave (RR) configurations. The last configuration corresponds to the regular reflection without a triple point. These regions are partially overlapped which indicates a possible nonuniqueness of the solution. Curve *4* separating vNR and MR corresponds to the T-configurations in which the flow is orthogonal to the reflected shock front. The reflected shock deflects the flow into the same direction, as the incident shock, in the vNR region and in the opposite direction in the MR region. The vNR region is remarkable by the fact that here the theoretical characteristics of the T-configurations are considerably different from those observed in the experiments.

As shown in [2], in the vNR region and in the upper part of the MR region the triple point proximity also contains a small-size singularity with high parameter gradients. The boundary of the existence of this singularity remained an open question. In [4] Guderley investigated this question in the potential flow approximation. In accordance with his results, the curvatures of the reflected front, the Mach front, and the streamline either vanish or increase without bounds at the triple point. In the interpretation of [12] this looks as follows. With respect to the flow entry angle β the shock waves can be subdivided into the strong family *A* and a weak family with supersonic flow behind the shock wave (family *C*) and a family with a subsonic flow. The lower boundary of the *A* family is the entry angle, at which the deflection angle reaches a maximum. The upper boundary of the *C* family is the entry angle, at which the Mach number behind the front is unity. There is a narrow region (family *B*) located between the *C* and *A* regions. If the reflected shock belongs to the *C* family, then the curvatures of the reflected front, the Mach front, and the streamline at the triple points are zero. If the reflected shock belongs to the *A* family, then the curvatures of the fronts and the streamline at the triple points are infinite and the singularity is similar with that in incompressible flow past a dihedral, that is, power-law in nature. The boundary of these regimes is within the narrow *B* family. The truth of these inferences for the ideal perfect gas model has not yet been verified.

The purpose of this study is to investigate the general properties and the differences in the triple point singularities in the GR, VR, vNR, and MR regions and to determine the boundary of the singularity existence in the MR region.

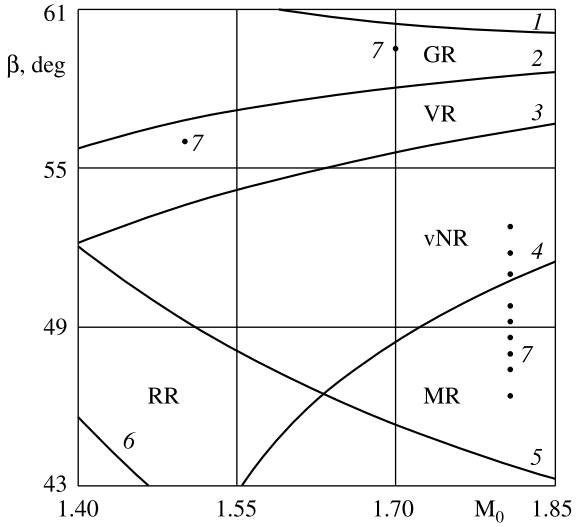

Fig. 2. Fragment of the diagram of the T-configuration regions in the case of steady shock wave reflection from a plane for a perfect gas with $\gamma = 5/3$; the configurations of Guderley (GR) in between (*1*) and (*2*), Vasil'ev (VR) (*2*, *3*), von Neumann (vNR) (*3*, *4*), and Mach (MR) below curve (*4*); regular reflection (RR) (*5*, *6*); (*7*) is the set of the calculated cases.

1. FORMULATION OF THE PROBLEM AND METHOD OF NUMERICAL SOLUTION

We will consider a plane supersonic steady flow of an ideal perfect gas in a channel with a rectilinear wedge. The wedge-produced shock wave is reflected from the opposite wall of the channel. The main flow elements in the case of irregular reflection are shown in Fig. 1, which presents the density contours in the representative calculations. At the triple point T the rectilinear incident-shock front is split into the reflected shock front above point T and the Mach front below this point. In the general case, both fronts are curvilinear. Apart from the shock waves, a contact discontinuity proceeds from point T and separates the flows having passed on either side of the triple point (in Fig. 1 it is visible as a condensation of the contours). On the edge of the reflecting wedge there is formed the centered expansion fan which intersects with the reflected shock front. On the weak shock range a subsonic flow is realized directly behind the Mach front and the reflected shock (shaded region in Fig. 1). However, further downstream the expansion wave transforms the subsonic flow into supersonic. The supersonic flow regime at the channel exit is the necessary condition of the realizability of this steady flow. If the narrow part of the channel is long, then multiple interactions of the reflected shock with the upper wall and the contact discontinuity can lead to the channel choking and the steady flow breakdown [13]. To eliminate the similar effects it is sufficient to consider channels with not too long narrow sections.

The relevant parameters of the problem are the oncoming flow Mach number M_0 and the angle of inclination of the incident shock β. At fixed wedge dimensions the flow also depends on the height L of the narrow section of the channel. In order for this flow could be realizable the channel height L must be greater than a certain minimum size L_m. A steady flow is possible only in the case in which $L \geq L_m$, when the reflected shock arrives at the wall to the right of the center of the expansion wave. To reduce the number of the input data in this study we considered configurations with the minimum height value $L = L_m$, that is, the configurations in which the reflected shock passes infinitely near from the center of the expansion wave. This makes the numerical simulation technology somewhat more difficult but reduces the number of the input parameters to two, namely, M_0 and β. Obviously that in these configurations the Mach front height is maximum.

In numerically modeling the flow the stationary solution was obtained by the stabilization method, that is, as a limiting time-dependent solution that has attained the steady state.

The differential equations governing the time-dependent two-dimensional flow of an inviscid and non-heat-conducting gas with constant specific heats are as follows:

$$\frac{\partial \mathbf{a}}{\partial t} + \frac{\partial}{\partial x}\mathbf{F}(\mathbf{a}) + \frac{\partial}{\partial y}\mathbf{G}(\mathbf{a}) = 0,$$

$$\mathbf{a} = \begin{bmatrix} \rho \\ \rho u \\ \rho v \\ e \end{bmatrix}, \qquad \mathbf{F}(\mathbf{a}) = \begin{bmatrix} \rho u \\ p + \rho u^2 \\ \rho uv \\ (e + p)u \end{bmatrix}, \qquad \mathbf{G}(\mathbf{a}) = \begin{bmatrix} \rho v \\ \rho uv \\ p + \rho v^2 \\ (e + p)v \end{bmatrix}, \tag{1.1}$$

$$e = \frac{p}{\gamma - 1} + \frac{1}{2}\rho(u^2 + v^2).$$

Here, x is the coordinate aligned with the lower reflecting plane, y is the coordinate orthogonal to x, ρ and p are the density and the pressure, u and v are the velocity components along the x and y axes, respectively, e is the total energy per unit volume, and the adiabatic exponent $\gamma = 5/3$.

The boundary conditions are those of impermeability at the channel walls and those of Rankine–Hugoniot at the shock waves. The flow parameters were normalized by the height of the narrow section of the channel and the speed of sound in the oncoming flow. In view of the fact that the flow region includes discontinuities, the required solution is considered to mean a weak solution satisfying the equations in the integral meaning.

The numerical solution was obtained using the baseline method [14] adapted to the case of curvilinear movable grids with an algorithm for fitting and tracing the shock fronts and the triple point [2].

The calculation technique consisted of two stages, namely, the calculation of the overall steady flow and an analysis of the flow in the vicinity of the triple point. In the first stage for given values of M_0 and β the overall steady flow was calculated at $L = L_m$. In this stage, the outer movable boundaries of the computation domain were the Mach front and the reflected shock front; in this case, the reflecting wedge edge with the center of the expansion fan was always located on the reflected shock front. Inside the computation domain the horizontal grid line proceeding from the triple point was adjusted with contact discontinuity shape. The calculations were performed by marching in time until the steady state of the flow pattern and the computation grid was attained.

In the second stage, the boundaries that were previously fixed (lower, upper, and right) start to continuously move toward the triple point with the conservation of similarity, so that the flow at the exit boundaries of the grid is supersonic relative to the grid. This approach makes it possible to avoid problems with the conditions at the boundaries of the grid contracting toward the triple point. At any moment of time the contracting grid is characterized by the contraction factor F_z which decreases from 1 to 0 in the contraction process. This technique performs simultaneously with tracing the main shock waves and the tangential discontinuity, which makes it possible to obtain with a high accuracy the quantitative information on the geometry of the discontinuity surfaces on all the contraction scales. We note that in this approach the calculations are always performed on the same movable grid. Any procedures of grid interpolation are not required.

To increase the accuracy and speed of calculations we also used the computation grid nonhomogeneity, the alternation of the contraction and stabilization stages, the stabilization accelerators, and the extrapolation of the initial conditions; the description of these procedures is beyond the scope of this paper. We only note that the contraction technique and the approaches mentioned above were earlier successfully employed in [9]. The main advantage of the technique described is that a set of unique calculations could be performed basing upon it for a finite time and with limited computational resources.

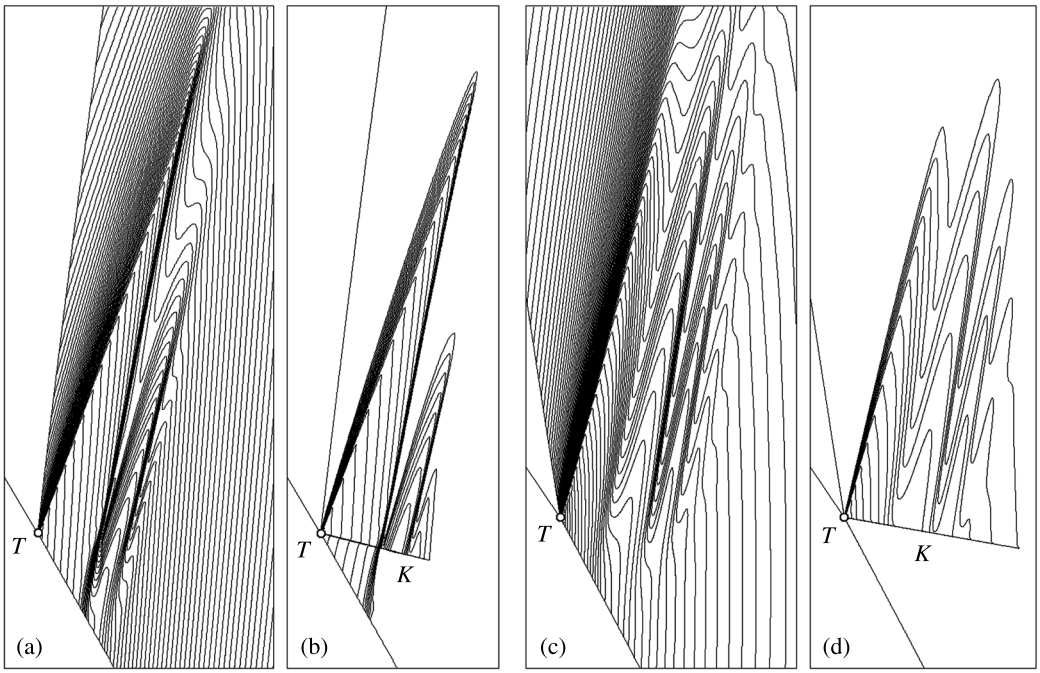

Fig. 3. Contours of the fragments of the pressure (a, c) and Mach number (M > 1) (b, d) fields near the triple point T; (a, b) GR case, $F_z = 8 \times 10^{-3}$, $\Delta p = 0.0004$, and $\Delta M = 0.0003$ and (c, d) VR case, $F_z = 4.5 \times 10^{-11}$, $\Delta p = 0.0002$, and $\Delta M = 0.0003$; K is the contact discontinuity.

2. RESULTS OF THE CALCULATIONS FOR GR AND VR

The calculations were performed for a perfect gas with the adiabatic exponent $\gamma = 5/3$ for the cases corresponding to the parameter ranges $\beta \in [46^\circ, 61^\circ]$ and $M_0 \in [1.38, 1.808]$. Here, only certain variants of the calculations are presented; in the diagram in Fig. 2 these are marked by bold points (*7*). The computation grid contained 640×800 points. In what follows, the calculated cases are called in accordance with the names of the regions, where they are located, namely, the GR case corresponding to $M_0 = 1.7$ and $\beta = 59.5^\circ$ and the VR case ($M_0 = 1.5$ and $\beta = 56.0^\circ$).

In Fig. 3 the pressure and Mach number contours for the GR and VR cases are plotted in the vicinity of the triple point. The Mach number contours are presented only in supersonic regions. From these contours the contact discontinuity position (K) is clearly traced. In both cases the cascade structure consisting of a sequence of supersonic zones can be observable. The final calculation stage of the grid contraction toward the triple point was terminated before the vertex of the local supersonic zone arrived at the upper boundary of the computation domain, which in Fig. 3 coincides with the upper boundary of the presented flowfield fragments. Clearly that the method does not generate any numerical artifacts on the upper boundary of the computation domain. The region of the supersonic zones shown in Fig. 3 included about 240×400 gridpoints. That was sufficient in order to identify three to four structures of the supersonic zone cascade, which can be well traced from the Mach number contours.

The distinctive features of these cases are the supersonic zone structures and dimensions. In accordance with the four-wave theory, in the second case the flow below the contact discontinuity is subsonic and the closing shocks penetrate there in the form of continuous smeared compression waves. An analogous behavior can be observable for the second closing shock in the first case. In this case the vertical dimensions of the supersonic zones and the closing shocks rapidly decrease. Each successive zone is half as large as the preceding one. In the second case the situation is different: the decrease proceeds more slowly and, moreover, the second zone is larger than the first one. This is due to the fact that the closing shock of the first zone has no time to form. The formation of the closing shocks, as the compression wave turnover, starts in the upper part of the expansion fans; they become stronger, as the contact discontinuity is approached. In

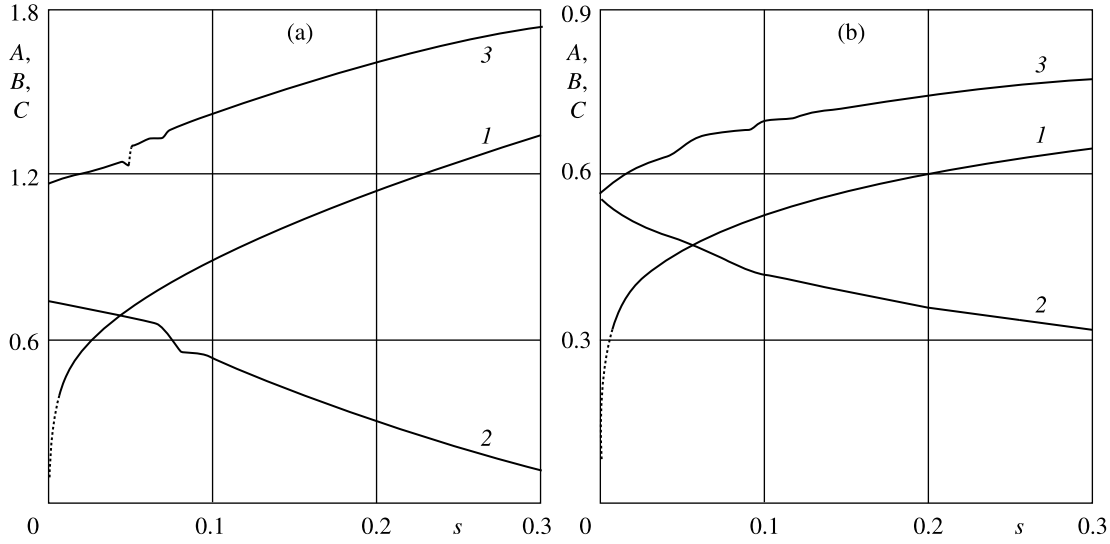

Fig. 4. Angles of inclination of the shock fronts and the tangential discontinuity in the vicinity of the triple point as functions of the normalized natural argument s; (a) GR case, $A(s) = \varphi_r(s) - 6^\circ$, $B(s) = \varphi_m(s) - 29^\circ$, and $C(s)/5 = \varphi_c(s) - 13.9^\circ$ and (b) VR case, $A(s) = \varphi_r(s) + 9.3^\circ$, $B(s) = \varphi_m(s) - 27.5^\circ$, and $C(s)/5 = \varphi_c(s) - 10^\circ$; (*1*) $A(s)$; (*2*) $B(s)$; and (*3*) $C(s)$.

the second case the closing shock is rather a continuous compression wave which has no time to be formed as a shock. We note that in [15] this factor of the delay in the intersection of characteristics was adduced as an argument in favor of the existence of a supersonic zone without closing shocks. Clearly that this is not the case. That the first closing shock could not be formed does not preclude the formation of the second and successive shocks.

In both GR and VR variants the linear dimensions of the supersonic zones differ by a factor of 10^8. For the first case the contraction factor $F_z = 8 \times 10^{-3}$, while for the second case $F_z = 4.5 \times 10^{-11}$. Obviously, the second structure is only an element of the solution of the mathematical ideal-gas model and is not realized in actual flows owing to its small dimensions.

The geometric characteristics of the shock fronts and the contact discontinuity for the two cases are presented in Fig. 4, in which the angles of inclination of the fronts to the coordinate axes are plotted against the natural parameter s measured along the front from the triple point. The angles of inclination to the vertical axis are presented for the shock waves (curves $A(s)$ and $B(s)$) and those to the horizontal axis are plotted for the contact (tangential) discontinuity (curves $C(s)$). The curves consist of separate points, any of which corresponding to one computation cell. The dimensionless natural parameter is normalized by F_z.

Clearly visible on the $C(s)$ curves are the splashes corresponding to the interactions between the closing shocks and the contact discontinuity. They make it possible to easily identify the belonging of the regions on the curves to particular parts of the flowfield fragments in Fig. 3. The analogous interactions can also be traced on the Mach fronts (curves $B(s)$). The derivatives of the curves plotted in Fig. 4 are proportional to the front curvatures. In both cases clearly visible is a large curvature of the reflected shock wave, which strongly increases, as the triple point is approached (that is, as $s \to 0$). For the Mach fronts and the tangential discontinuities this behavior is not observable: the curvatures of these fronts remain finite up to the triple point. Moreover, in the GR case the dependences near $s = 0$ are near-linear, that is, the corresponding sections of the fronts are similar in shape with circular arcs. In the GR case the Mach front curvature reaches a maximum outside the supersonic zone, while in the VR case its maximum is at the triple point. We recall that in the VR case the flow behind the Mach front is subsonic. We also note that in the VR case the gradients and curvatures, though finite, can be very large due to the smallness of the singularity dimensions. Thus, the actual ranges of the argument variation in Fig. 4a and 4b are proportional to F_z and differ by a factor of 10^8.

The finiteness of the front curvatures is accompanied by the finiteness of the parameter gradients in these zones. Thus, in the GR and VR cases the singularity with infinite gradients is concentrated only in a narrow subsonic zone between the reflected front and the expansion fan. In the other regions the singularity does not manifest itself. This fact was noted in [1] but later it was questioned in [2]. The results presented above indicate that the original standpoint was more adequate.

3. RESULTS OF THE CALCULATIONS FOR vNR AND MR

The results that follow pertain to the transitional region between vNR and MR for the same adiabatic exponent $\gamma = 5/3$. The MR region borders with the RR region along curve *5* in Fig. 2. Below this curve there is the possibility of the existence of a solution in the form of regular reflection. The possibility of the Mach reflection is also conserved. Theoretically, in this region the solution can be two-valued. The realization of one or another regime depends on the complete formulation of the problem and, in particular, on the downstream conditions.

As applied to the given problem of reflection in a plane channel, the Mach-to-regular transition on the range of weak shock waves was investigated for the Mach numbers $M_0 = 1.5$ and 1.808. The calculated dependences of the front height in the steady flow with a gradually decreasing angle of the incident shock inclination β are plotted in Fig. 5a. In this figure $\beta_R = \beta_R(M_0)$ is the limiting angle of the incident shock inclination in the case of the regular reflection. Curves *3* in Fig. 5a are the results of the quadratic interpolation which show that the Mach front height vanishes, as the regular reflection boundary is approached, that is, transition to the regular reflection occurs precisely at the $\beta = \beta_R(M_0)$ boundary. We note that, when the problem conditions, for example, the lower wall shape, are varied, the irregular reflection can also exist below this boundary.

To determine the boundary of the singularity existence at the triple point on transition from the vNR to the MR region we performed the calculations for the governing parameters from the ranges $M_0 = 1.808$ and $\beta \in [46.6^\circ,\ 52.8^\circ]$. The points corresponding to these range are marked in Fig. 2. It was found that the singularity is present in all these cases and it does not vanish, as the regular reflection boundary is approached. The reflected front geometry $\varphi_r(s)$ is similar with the $A(s)$ curves in Fig. 4. To illustrate this fact in compact form in Fig. 5b we have plotted the differences $\varphi_r(s) - \varphi_r(0)$ for different values of s against the angle β measured from β_R. The quantity $\varphi_r(0)$ is the angle of the reflected front inclination directly at the triple point and $\varphi_r(s)$ is the angle of inclination at a point on the front at a distance s from the triple point. Thus, for example, in the vicinity of the triple point, $10^{-4}L_m$ in size, which is smaller than the resolution limits in the existing laboratory measurements, the angle of the reflected front inclination varies by 1 to 3 degrees. The extrapolation (*3*) in Fig. 5b indicates that the reflected front singularity at the triple point is conserved up to transition to the regular reflection.

In Fig. 6 the analogous dependences are plotted for the Mach front and the tangential discontinuity. Here, the same tendency can be observable, though with somewhat smaller angle variations in the vicinity of the triple point. Thus, as distinct from the GR and VR cases considered above, in vNR and MR the Mach front and the tangential discontinuity have infinite curvature at the triple point, which is in agreement with Guderley's results [4].

In [3] basing upon the properties of numerical solutions a formula was derived that demonstrates that in GR the reflected front shape has the logarithmic singularity

$$\varphi_r(s) = \varphi_r(0) - \frac{D(M_0,\ \beta)}{\lg(s/s_0)}, \tag{3.1}$$

where the coefficient D depends on the initial data of the reflection and a certain scale length $s_0 \gg s$.

In Fig. 7 the validity of this dependence for the reflections is checked in the vNR and MR cases. The quantity $s_0 = L_m$ is taken for the scale length. In this case, the argument under the logarithm sign is the dimensionless natural parameter. In Fig. 7 the calculated dependences of the angles of the reflected front

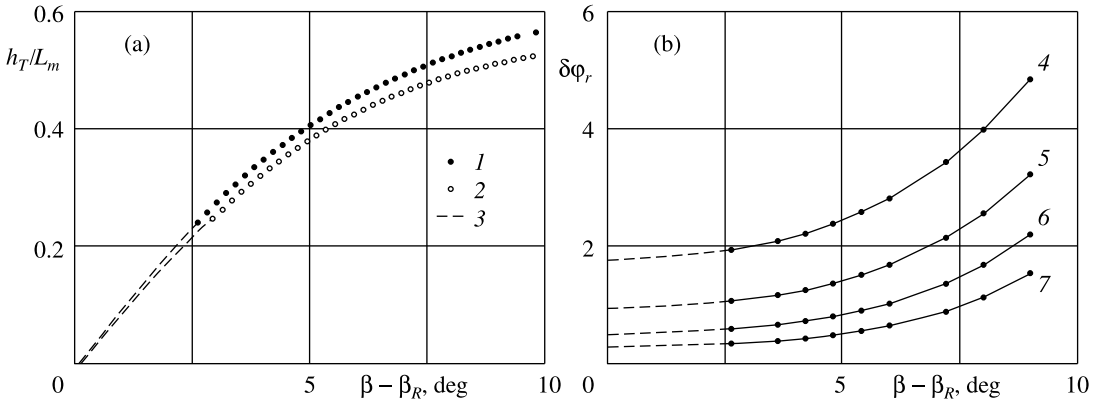

Fig. 5. Dependences of the Mach front height (a) and the angles of the reflected front inclination (b) on the angle of the incident shock inclination; β_R is the limiting angle of the regular reflection; $M_0 = 1.808$ (*1*) and 1.5 (*2*); (*3*) is extrapolation; $\delta\varphi_r = \varphi_r(s) - \varphi_r(0)$; $s = 10^{-3}$, 10^{-4}, 10^{-5}, and 10^{-6} (*4–7*).

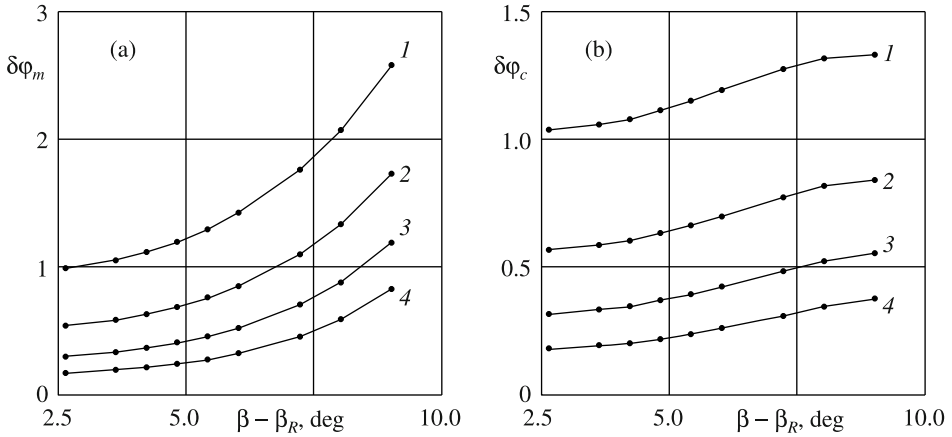

Fig. 6. Dependences of the angles of inclination of the Mach front (a) and the tangential discontinuity (b) on the angle of the incident shock inclination; β_R is the limiting angle of the regular reflection; $\delta\varphi = \varphi(s) - \varphi(0)$; $s = 10^{-3}$, 10^{-4}, 10^{-5}, and 10^{-6} (*1–4*).

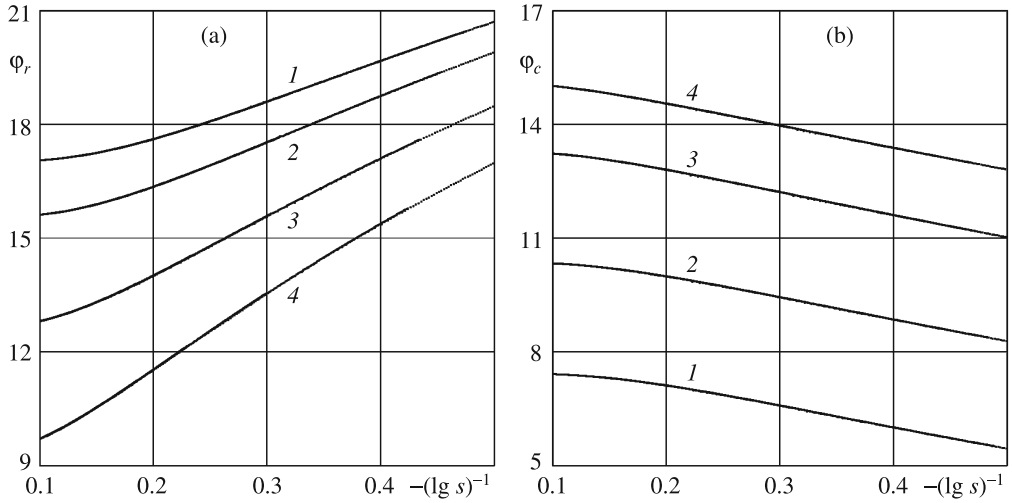

Fig. 7. Angles of inclination of the reflected shock wave (a) and the tangential discontinuity (b) near the triple point as functions of the logarithmic argument; $M_0 = 1.808$ and $\beta = 46.4°$, $48.6°$, $51°$, and $52.8°$ (*1–4*).

inclination are presented as functions of the logarithmic argument $-(\lg s)^{-1}$ for four variants. The s range is $10^{-10} < s < 10^{-2}$. The curves are composed of the data of eight successive calculations with different values of $F_z = 10^{-1} \to 10^{-8}$. The grids of these calculations are partially overlapping. Despite the fact that the result for any cell is presented as a discrete point, the totality of the points looks as a bold curve. The junctions of neighboring calculations can be seen at the upper parts of curves *2–4* in Fig. 7a. Generally, the transition zones are almost indistinguishable, which indicates the high efficiency and adequate realization of the calculation technique.

For all the curves on the $10^{-5} < s < 10^{-2}$ range the logarithmic dependence is near-linear; for the tangential discontinuity the proportionality coefficient D is almost independent of the angle β. In this small vicinity of the triple point the angle of the tangential discontinuity inclination varies by 2° as minimum. The analogous variations for the reflected front are several times greater and the dependence of the proportionality coefficient D on the input parameter β manifests itself fairly clearly. These differences in the front geometries indicate that the singularity in the sector between the reflected front and the tangential discontinuity is inhomogeneous with respect to directions. If an approximation for the analytical solution in the vicinity of the triple point is sought in the form similar with (3.1), then the dependence of the coefficients of the logarithms on the polar angle should be allowed. From the plots in Fig. 7 it can also be seen that with further approach to the triple point, that is, at $10^{-10} < s < 10^{-5}$, the linearity changes for a dependence which is nearer to quadratic. All these facts indicate a complicated structure of the singular solution, which possesses a greater number of degrees of freedom than the solution with finite gradients. We note that the logarithmic nature of the singularity differs from the power-law behavior obtained by Guderley in the potential approximation.

With increase in M_0 the singularity amplitude gradually diminishes. An attempt to determine the M_0 range of singularity existence has been unsuccessful. It was only established that the singularity conserves up to $M_0 = 2$.

4. DISCUSSION

We note that within the framework of the ideal perfect gas model the singularity at the triple point in the MR case can be explained fairly simply. In fact, let us assume that the flow parameter gradients and the front curvatures are finite at the triple point and the three-wave theory works, which includes a closed system of equations at the shock waves and the tangential discontinuity. Then the passage to the triple point limit in Eqs. (1.1) and the differential relations following from the conditions at discontinuities yield a system of 18 linear homogeneous equations in 18 unknowns, namely, two curvatures of the reflected front and the Mach front and 16 components of the gradients in the sectors behind the shock waves. For a nonzero solution to exist the determinant of the system should be zero. In the general case, this additional condition is inconsistent with the three-wave theory equations, that is, a solution with finite nonzero gradients does not exist. Instead of this solution, there appears a solution with a gradient singularity at the triple point. We note that the above considerations do not exclude the existence of T-configurations with zero curvatures of the shock waves and zero gradients, which were allowed by Guderley. In this case, the singularity exhibits itself only in the second derivatives of the solution. At $M_0 \le 2$ these T-configurations were not observable.

If the flow behind the reflected shock is supersonic, then the condition on the going-away characteristics should be excluded from the equations of motion and the system that remained can admit a solution with finite nonzero gradients. The consideration of the previous paragraph can be inapplicable for triple points in axisymmetric or self-similar flows, since in this case the equations of motion include source terms, which leads to inhomogeneous systems of equations with respect to the gradients.

As for self-similar solutions, the double Mach reflection at $\gamma = 1.4$ was considered in detail in [16], in which case the second triple point includes a singularity. It is noteworthy that in [16] and in the equivalent T-configuration for the problem of stationary reflection ($M_0 = 2.2$, $\beta = 47°$) the curvatures of the shock waves and the tangential discontinuity are opposite in sign. This means that the subsonic singularity pa-

rameters cannot be uniquely determined from the local theory and adapt to the global flow. The singularity plays the role of a sort of a versatile mechanism of the smooth matching of the local solution provided by the three-wave theory and the global solution. Then a conclusion suggests itself that on the range of moderately weak shock waves the presence of singularity at the triple point of the triple configuration with subsonic flow on either side of the tangential discontinuity is rather a rule than an exception.

Summary. Detailed calculations of flows in the vicinity of triple points are performed in the case of the stationary irregular reflection of weak and moderate shock wave using a new numerical method. The results of the calculations show that in the case in which the four-wave flow pattern is realized, the curvatures of the tangential discontinuity and the Mach front are finite at the triple point. In this case, the singularity with infinite gradients is concentrated only in the sector in between the reflected shock front and the expansion fan. When the three-wave flow pattern is realized, the curvatures of the tangential discontinuity and the both shock fronts are infinite at the triple point. On the range of weak and moderate shock waves the logarithmic singularity in the subsonic sectors near the triple point conserves up to transition to the regular reflection.

REFERENCES

1. E. I. Vasil'ev, "High-Resolution Simulation for the Mach Reflection of Weak Shock Waves," in: *Proc. ECOMAS CFD 1998, Vol. 1, Pt. 1*, Wiley, Hoboken (1998), p. 520.
2. E. I. Vasil'ev and A. N. Kraiko, "Numerical Modeling of Weak Shock Diffraction on a Wedge under the von Neumann Paradox Conditions," Zh. Vychisl. Mat. Mat. Fiz. **39**, 1393 (1999).
3. E. I. Vasil'ev, "Four-Wave Scheme of Weak Mach Shock Wave Interaction under von Neumann Paradox Conditions," Fluid Dynamics **34** (3), 421 (1999).
4. K. G. Guderley, "Considerations of the Structure of Mixed Subsonic-Supersonic Flow Patterns," Wright Field Report F-TR-2168-ND (1947), p. 144.
5. B. W. Skews and J. T. Ashworth, "The Physical Nature of Weak Shock Wave Reflection," J. Fluid Mech. **542**, 105 (2005).
6. B. W. Skews, G. Li, and R. Paton, "Experiments on Guderley Mach Reflection," Shock Waves **19**, 95 (2009).
7. A. Cachucho and B. W. Skews, "Guderley Reflection for Higher Mach Numbers in a Standard Shock Tube," Shock Waves **22**, 141 (2012).
8. A. M. Tesdall, R. Sanders, and B. L. Keyfitz, "Self-Similar Solutions for the Triple Point Paradox in Gasdynamics," SIAM J. Appl. Math. **68**, 1360 (2008).
9. E. I. Vasilev, "Detailed Investigation of Guderley Shock Wave Reflections in Steady Flow," in; *Proc. 21st Int. Shock Interaction Symp., Latvia, 3–8 Aug. 2014*, Univ. Latvia, Riga (2014), p. 42.
10. A. M. Tesdall, R. Sanders, and N. Popivanov, "Further Results on Guderley Mach Reflection and the Triple Point Paradox," J. Scientific Computing **64**, 721 (2015).
11. G. Ben-Dor, *Shock Wave Reflection Phenomena*, Springer, New York (2007).
12. J. Sternberg, "Triple-Shock-Wave Intersections," Phys. Fluids **2** (2), 179 (1959).
13. G. Ben-Dor, T. Elperin, H. Li, E. Vasiliev, A. Chpoun, and D. Zeitoun, "Dependence of Steady Mach Reflection on the Reflecting-Wedge Trailing-Edge Angle," AIAA J. **35**, 1780 (1997).
14. E. I. Vasil'ev, "W-Modification of the Godunov Method and its Application to Time-Dependent Two-Dimensional Dusty Gas Flows," Zh. Vychisl. Mat. Mat. Fiz. **36**, 122 (1996).
15. E. I. Vasilev, T. Elperin, and G. Ben-Dor, "Analytical Reconsideration of the von Neumann Paradox in the Reflection of a Shock Wave over a Wedge," Phys. Fluids **20**, 046101 (2008).
16. L. F. Henderson, E. I. Vasilev, G. Ben-Dor, and T. Elperin, "The Wall-Jetting Effect in Mach Reflection: Theoretical Consideration and Numerical Investigation," J. Fluid Mech. **479**, 259 (2003).